Guidance and Control of Unmanned Surface Vehicles via HEOL

Loïck Degorre, Emmanuel Delaleau, Cédric Join, Michel Fliess

Available online at www.sciencedirect.com

ScienceDirect

IFAC Papers Online CONFERENCE PAPER ARCHIVE

IFAC PapersOnLine 59-12 (2025) 13–18

Guidance and Control of Unmanned Surface Vehicles via HEOL

Loïck Degorre * **Emmanuel Delaleau** ** **Cédric Join** ***,‡ **Michel Fliess** ****,†,‡

* *ENSTA, UMR 6285, IPP Lab-STICC, 29 200 Brest, France.* loick.degorre@ensta.fr

** *ENI Brest, UMR CNRS 6027, IRDL, 29 200 Brest, France.* emmanuel.delaleau@enib.fr

*** *CRAN (CNRS, UMR 7039), Université de Lorraine, Campus Aiguillettes, BP 70239, 54506 Vandœuvre-lès-Nancy, France.* cedric.join@univ-lorraine.fr

**** *LIX (CNRS, UMR 7161), École polytechnique, 91128 Palaiseau, France.* michel.fliess@polytechnique.edu

† *LJLL (CNRS, UMR 7238), Sorbonne Unversité, 75005 Paris, France* michel.fliess@sorbonne-universite.fr

‡ *AL.I.E.N., 7 rue Maurice Barrès, 54330 Vézelise, France.* {cedric.join, michel.fliess}@alien-sas.com

Abstract: This work presents a new approach to the guidance and control of marine craft via HEOL, i.e., a new way of combining flatness-based and model-free controllers. Its goal is to develop a general regulator for Unmanned Surface Vehicles (USV). To do so, the well-known USV maneuvering model is simplified into a nominal Hovercraft model which is flat. A flatness-based controller is derived for the simplified USV model and the loop is closed via an intelligent proportional-derivative (iPD) regulator. We thus associate the well-documented natural robustness of flatness-based control and adaptivity of iPDs. The controller is applied in simulation to two surface vessels, one meeting the simplifying hypotheses, the other one being a generic USV of the literature. It is shown to stabilize both systems even in the presence of unmodeled environmental disturbances.

Keywords: Autonomous vehicles, Nonlinear systems, Algebraic/geometric methods.

1. INTRODUCTION

With the increasing number of applications for both surface and underwater autonomous vehicles, a great number of control methods and guidance principles have been developed in recent years, but the need for efficient and robust trajectory-tracking controllers yet remains. In this work, surface vessels are considered as a reduced case of underwater vehicles constrained in the horizontal plane. They are used as a first step towards the design of all-purpose controllers for underwater craft.

Control of under-actuated surface vehicles has been addressed in different manners but mostly for path following and path tracking applications. See (Pettersen and Nijmeijer (1998); Breivik and Fossen (2005); Elmokadem et al. (2016)) for some of the most common methods, and (Degorre et al. (2023)) for a survey.

In the present work, control of the *Unmanned Surface Vehicle* (*USV*) is addressed with the HEOL setting, a very interesting candidate for control of marine craft because of its robustness and adaptability. In order to use this flatness-based method, a simplified, flat nominal model is extracted from the USV conventional maneuvering model and is used to establish the controller. This simple model is similar to the *Hovercraft* model which is naturally flat (see Sira-Ramírez and Agrawal (2004); Degorre (2023), and the references therein for details).

The so-obtained guidance principle is then applied to standard USVs and, because of the robustness of the method, displays good performance in trajetcory tracking tasks.

This work illustrates the efficiency of *HEOL* (Join et al. (2024)), which combines in a new manner the well-known *Flatness-Based Control* (Fliess et al. (1995, 1999)) with *Model-Free Control* (*MFC*) (Fliess and Join (2013, 2022)) and the corresponding *intelligent* controllers. Note that HEOL has already been illustrated by Delaleau et al. (2025) and Join et al. (2025). One should however not forget that

- many concrete case-studies have employed MFC since almost twenty years: see, e.g., Gédouin et al. (2011) and Artuedo et al. (2024) among a large list of references;
- the connection between flatness and MFC has a long history: see, e.g., Scherer et al. (2023) for a recent reference.

10.1016/j.ifacol.2025.09.560

In HEOL the *ultra-local model* (Fliess and Join (2013)) is replaced by a *homeostat*, which allows the coefficients of the control variables to be obtained immediately. Here an *intelligent proportional-derivative controller* (*iPD*) (Fliess and Join (2013, 2022)) is used. The *data-driven* term, which helps compensating disturbances and mismatches, is obtained via algebraic estimation techniques (Fliess and Sira-Ramírez (2003)).

The paper is organized as follows. Sect. 2 recalls the models of both the surface vessel and the hovercraft. Sect. 3 sketches the proof of flatness of the hovercraft model. Sect. 4 develops the iPD. Sect. 6 draws some conclusions.

2. MODEL OF THE VEHICLE

This section introduces the model of the surface vessel and describes the simplifying hypotheses leading to the hovercraft model. The models are derived from the well-known surface vessel maneuvering model described in Fossen (2021).

In this work, the simplified USV, thereafter called "hovercraft" for simplicity, is considered to be a surface vessel with a circular hull-shape and homogeneous mass distribution. The added mass and damping parameters are then equal in surge and sway. This hypothesis does simplify the surface vessel model, notably making the yaw dynamics of the vehicle independent of the surge and sway dynamics.

Both models are constrained to the horizontal plane and both vehicles are considered to be actuated with two parallel thrusters generating independent surge force τ_u and yaw moment τ_r. They are then ill-actuated with respect to the positioning tasks at hand, and a guidance principle is mandatory (Degorre (2023)).

2.1 Surface vessel model

To establish the model of a surface marine vessel, one needs to consider two different frames: the earth-fixed *inertial frame* $\mathcal{R}_0(\boldsymbol{O_o}, \boldsymbol{x_o}, \boldsymbol{y_o}, \boldsymbol{z_o})$ and the *body-fixed* frame $\mathcal{R}_B(\boldsymbol{O_B}, \boldsymbol{x_B}, \boldsymbol{y_B}, \boldsymbol{z_B})$ centered on the center of gravity of the vehicle and rotated of an angle ψ around $\boldsymbol{z_o}$ w.r.t. $\mathcal{R}_0$. The variables that appear in the model are: x, y the coordinates of the vehicle in $\mathcal{R}_0$, the translation speed components u, v in $\mathcal{R}_B$, the heading angle of the hovercraft ψ, the rotation speed r of $\mathcal{R}_B$ w.r.t. $\mathcal{R}_0$. The controls are F_u, the propulsion force, and Γ_r, the rotating moment normalized in mass. The surface vessel model is:

$$\dot{x} = u\cos\psi - v\sin\psi \tag{1a}$$
$$\dot{y} = u\sin\psi + v\cos\psi \tag{1b}$$
$$\dot{\psi} = r \tag{1c}$$
$$\dot{u} = F_u + avr - \beta_u u \tag{1d}$$
$$\dot{v} = bur - \beta_v v \tag{1e}$$
$$\dot{r} = \Gamma_r + cuv - \gamma r \tag{1f}$$

the details about the coefficients $a, b, c, \beta_u, \beta_v, \gamma$ are given in the Appendix.

2.2 Hovercraft model

The hovercraft dynamic model is established using the surface vessel model (1) and considering a circular hull shape. The mass ratios a, b and c thus become: $a = 1$, $b = -1/a = -1$, $c = 0$. In the same way, the surge and sway damping contributions β_u and β_v are equivalent. Thus: $\beta_u = \beta_v = \beta$.

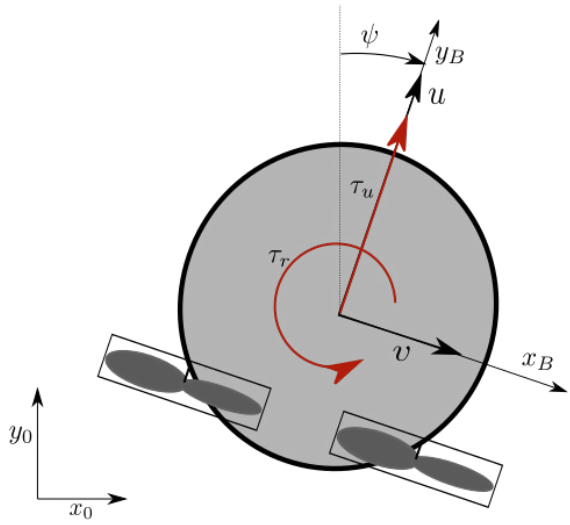

Fig. 1. Schematic representation of the hovercraft.

With these hypotheses, the kinematic part of the model, (1a) to (1c), is not modified, and the surface vessel model becomes:

$$\dot{x} = u\cos\psi - v\sin\psi \tag{2a}$$
$$\dot{y} = u\sin\psi + v\cos\psi \tag{2b}$$
$$\dot{\psi} = r \tag{2c}$$
$$\dot{u} = F_u + vr - \beta u \tag{2d}$$
$$\dot{v} = -ur - \beta v \tag{2e}$$
$$\dot{r} = \Gamma_r - \gamma r \tag{2f}$$

Note that because of the shape hypothesis, the yaw dynamics described by Eq. (2f) are independent of the surge and sway modes of the vehicle.This assumption is obviously not met in practice on generic surface vessels.

3. FLATNESS OF THE HOVERCRAFT MODEL

3.1 Preliminary remark

While the surface vessel model (1) is notoriously not flat , the hovercraft model is flat with the flat output $\boldsymbol{z} = [x, y]^\top$ (Sira-Ramírez and Agrawal (2004)). The flatness proof is briefly recalled here and the reader is referred to (Sira-Ramírez (2002); Rigatos (2015); Degorre (2023)) for more details.

3.2 Proof

Set

$$\psi = \arctan\left(\frac{\ddot{y} + \beta\dot{y}}{\ddot{x} + \beta\dot{x}}\right) \tag{3}$$

Deriving ψ in Eq. (3) yields the yaw velocity r and the normalized yaw moment Γ_r:

$$r = \dot{\psi}, \quad \Gamma_r = \ddot{\psi} + \gamma\dot{\psi}$$

The heading angle expression (3) unlocks expressions of the surge and sway velocities, as well as the surge force:

$$u = \dot{x}\cos\psi + \dot{y}\sin\psi \tag{4}$$
$$v = -\dot{x}\sin\psi + \dot{y}\cos\psi \tag{5}$$
$$F_u = (\ddot{x} + \beta\dot{x})\cos\psi + (\ddot{y} + \beta\dot{y})\sin\psi \tag{6}$$

The hovercraft (2) has been shown to be flat with flat output $\boldsymbol{z} = [x, y]^\top$.

3.3 Brunovský representation

For simplicity, considering the hovercraft model (2), a first change of input is performed. Because the yaw dynamics described by (2c) and (2f) are decoupled from the position dynamics, one can proceed to considering the yaw angle ψ as an input of the system instead of the yaw moment Γ_r. This change of input is equivalent to assuming that an additional control stage with much faster converging dynamics ensures that the heading angle is almost instantaneously stabilized to the reference value calculated by the flatness-based guidance principle. This is a common assumption in marine robotics when developing guidance principles (Mitchell et al. (2003); Breivik and Fossen (2005)).

Then, in order to retrieve the Brunovský-like formulation (Delaleau and Rudolph (1998); Hagenmeyer and Delaleau (2003a)) of the system composed of two independent integrator chains, a second change of input is performed. The system to control thus becomes:

$$\dot{x} = v_x \tag{7a}$$
$$\dot{v}_x = w_x \tag{7b}$$
$$\dot{y} = v_y \tag{7c}$$
$$\dot{v}_y = w_y \tag{7d}$$

with the two new inputs w_x and w_y defined as:

$$w_x = F_u\cos\psi - \beta v_x \tag{8a}$$
$$w_y = F_u\sin\psi - \beta v_y \tag{8b}$$

The original inputs of the system can be obtained with:

$$\psi = \arctan\left(\frac{w_y + \beta v_y}{w_x + \beta v_x}\right) \tag{9a}$$
$$F_u = (w_x + \beta v_x)\cos\psi + (w_y + \beta v_y)\sin\psi \tag{9b}$$

Remark 1. The singularity introduced in (9) because of the change of input can be overcome using the well known *arctan2* function and additional usual strategies. Reference trajectories of the task can also be chosen to avoid any singularities. See Degorre et al. (2023) for a precise recall of the *arctan2* function.

Remark 2. An additional control stage is necessary to ensure that the heading angle of the vehicle does converge towards the reference value calculated with the guidance principle introduced in the following. As it is often the case with the conventional *Guidance-Control* structure used with autonomous vehicles, the HEOL approach presented in this work leads to a *cascade system*. A standard PID or Sliding Mode controller would be suited to ensure stability of the lower level, provided it is faster than the outer loop. The cascade system is depicted on Fig. 2. Note also that many autonomous vehicles, especially commercial USVs, feature an embedded autopilot ensuring stability of the lower level of the cascade.

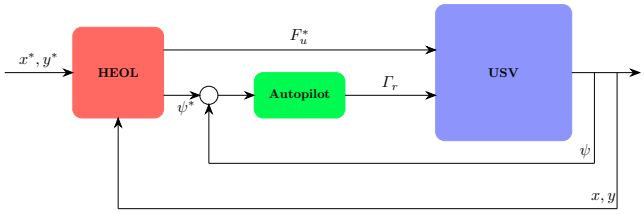

Fig. 2. Cascade structure

4. DESIGN OF THE CONTROLLER

In this section, the controller combining flatness and model-free control is designed. It associates the natural robustness of flatness-based control and exact feedforward linearization Hagenmeyer and Delaleau (2003b) with the adaptivity of Model-Free Control Fliess and Join (2013). The controller is based on the very simple hovercraft model in the inertial frame (7) and is meant to be applied to the more complex surface vessel.

The controller is composed of a nominal control calculated in a feedforward linearizing fashion Hagenmeyer and Delaleau (2003a) and of an Intelligent Proportional Derivative regulator used to close the loop. The contributions of the nominal controls and the iPDs regulators are linearly summed in the controller. In this case, the robustness and adaptivity of the iPDs allow compensating the mandatory model approximations required for the design of the flatness-based guidance principle.

4.1 Nominal Controls

In an exact feedforward linearizing fashion, nominal values of the controls are computed using the equations of the Brunovský form obtained with flatness. Recalling 7b and 7d, one gets the nominal controls:

$$w_x^* = \dot{v}_x^* = \ddot{x}^* \tag{10a}$$
$$w_y^* = \dot{v}_y^* = \ddot{y}^* \tag{10b}$$

where x^*, y^* and their derivatives denote desired values issued from the trajectory.

4.2 Closed-loop control design

Set

$$w_x = w_x^* - \Delta w_x$$
$$w_y = w_y^* - \Delta w_y$$

It yields

$$\ddot{e}_x = \Delta w_x, \quad e_x = w_x^* - w_x$$
$$\ddot{e}_y = \Delta w_y, \quad e_y = w_y^* - w_x$$

and, according to Join et al. (2024), the *homeostat*

$$\begin{aligned}\ddot{e}_x &= F_x + \Delta w_x\\ \ddot{e}_y &= F_y + \Delta w_y\end{aligned} \tag{11}$$

where F_ζ, $\zeta = x, y$, accounts for the mismatches and disturbances. Following Fliess and Join (2022), an estimate $\widehat{F}_\zeta$ of F_ζ reads

$$\begin{aligned}\widehat{F}_\zeta(t) = \frac{60}{T^5}\int_0^T \Big[\Big((T-\sigma^2) - 4(T-\sigma)\sigma + \sigma^2\Big)e_\zeta(\sigma + t - T)\\ + \frac{1}{2}(T-\sigma)^2\sigma^2\Delta w_\zeta(\sigma + t - T)\Big]d\sigma\end{aligned} \tag{12}$$

The corresponding *intelligent proportional-derivative controller* (*iPD*) reads

$$\Delta w_\zeta = -\left(K_p e_\zeta + K_d \dot{e}_\zeta + \widehat{F}_\zeta\right) \tag{13}$$

where $K_p, K_d \in \mathbb{R}$ are constant gains, such that the polynomial $s^2 + K_d s + K_p$ is Hurwitz.

Riachy's trick (Fliess and Join (2022)) permits to avoid the calculation of the derivative $\dot{e}_\zeta$. Rewrite (11) as $\ddot{e}_\zeta + K_d \dot{e}_\zeta = F(t) + K_d \dot{e}_\zeta + \Delta w_\zeta$. Set

$$Y_\zeta(t) = e_\zeta(t) + K_d \int_c^t e_\zeta(\sigma) d\sigma, \quad 0 \leqslant c < t$$

It yields $\dot{Y}_\zeta = \ddot{e}_\zeta + K_d \dot{e}_\zeta$. Set $\mathcal{F}_\zeta = F_\zeta + K_d \dot{e}_\zeta$. Eqn. (11) becomes $\dot{Y}_\zeta = \mathcal{F}_\zeta + \Delta w_\zeta$. Eqn. (13) reads now

$$\Delta w_\zeta = -(\widehat{\mathcal{F}}_\zeta + K_p e_\zeta) \tag{14}$$

where the derivative of e_ζ disappears. The estimate $\widehat{\mathcal{F}}$ in Eqn. (14) may be computed via Formula (12) by replacing e_ζ by Y_ζ.

Set

- $K_p^x = K_p^y = K_p$;
- $K_d^x = K_d^y = K_d$.

and only two parameters remain to tune, namely K_p and K_d. At last, the inputs of the Brunovský equivalent system are:

$$w_x = \ddot{x}^* + K_d \dot{e}_x + K_p e_x - \widehat{F}_x \tag{15a}$$

$$w_y = \ddot{y}^* + K_d \dot{e}_y + K_p e_y - \widehat{F}_y \tag{15b}$$

For added robustness, the original inputs of the simplified hovercraft system are reconstructed in a feedforward linearizing fashion (Hagenmeyer and Delaleau (2003b)):

$$\psi = \arctan\left(\frac{w_y + \beta \dot{x}^*}{w_x + \beta \dot{y}^*}\right) \tag{16a}$$

$$F_u = (w_x + \beta \dot{x}^*)\cos\psi + (w_y + \beta \dot{y}^*)\sin\psi \tag{16b}$$

The additional control stage used for tracking of the ψ reference calculated by the controller can either be a very simple PID or SMC or a commercial autopilot system.

Overall, the flatness of the simplified hovercraft system allows designing a flatness-based guidance principle, calculating a surge control force and a yaw angle reference out of the position measurements. Then, iPDs are used to close the loop in an adaptive manner, compensating the model approximations of the hovercraft and any unmodeled disturbance.

5. SIMULATION RESULTS

The controller associating flatness and model-free control is tested in simulation in two different scenarios. First, it is tested on a hovercraft in the presence of a constant disturbing force similar to the force of wind. In this case, the algebraic estimators associated to the iPDs compensate the disturbing effect of the wind. Then, the controller is evaluated on a surface vessel similar to the *Otter* USV (*Maritime Robotics*, see : `https://www.maritimerobotics.com/otter`). This vehicle does not meet the hovercraft simplifying hypothesis. It is evaluated on a circular trajectory in the with the same disturbing external force.

5.1 Control of the hovercraft

In this first example, the controller is tested on the hovercraft with an external disturbing wind force. The vehicle has a circular hull and thus $a = 1$, $b = -1$ the normalized damping parameter is chosen as $\beta = 10$. The wind is simulated as a constant normalized force in the inertial frame. It is aligned with the $\boldsymbol{y_o}$-axis with a normalized magnitude equal to -50.

The hovercraft is tested on a simple straight segment defined as $x^*(t) = 2t$, $y^*(t) = 0$. It is initiated with a 10m initial error on the $\boldsymbol{y_o}$ axis.

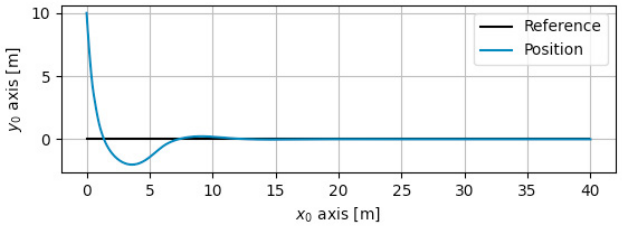

Fig. 3. Trajectory of the hovercraft in the $(\boldsymbol{x_o}, \boldsymbol{y_o})$ plane, in presence of a wind force aligned with the $\boldsymbol{y_o}$ axis. Black: Reference trajectory - Blue: Actual trajectory of the vehicle

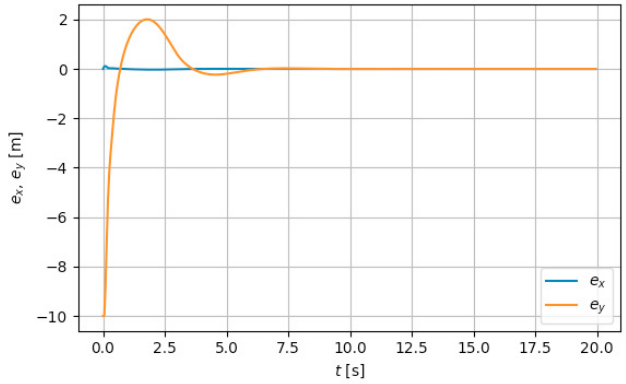

Fig. 4. Tracking errors of the hovercraft over time. Blue: Error on the $\boldsymbol{x_o}$ axis - Orange: Error on the $\boldsymbol{y_o}$ axis

Figs. 3 and 4 display the behavior of the vehicle and of the tracking errors on this task. Even with the considerable initial error, both errors converge to zero rapidly.

Fig. 5 shows that the $\boldsymbol{y_o}$-axis estimator F_y does converge towards the disturbing force while F_x stays around zero. This figure confirms that without model approximations, the estimators of the iPDs behave like the integral terms of conventional PIDs and compensate the unmodeled disturbance.

This first example shows that, on the very simple task of tracking line with a hovercraft, the controller behaves as expected. The estimators compensate all disturbing effects and the allow tracking without steady state error.

5.2 Control of a standard USV

In this second example, the controller is applied to a USV similar to the *Otter* USV (the parameters are derived from

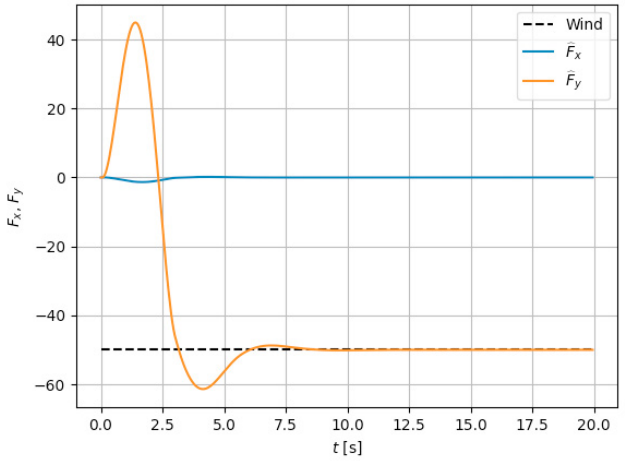

Fig. 5. Estimated values of F_x and F_y over time for the hovercraft. Dashed Black: Wind force - Blue: $\widehat{F}_x$ - Orange:$\widehat{F}_y$

Fossen and Perez (2004)). On this vehicle the parameters are:

$$a = 0.58, \quad b = -1.72, \quad \beta = \beta_u = 10, \quad \beta_v = 1.5\beta$$

The vehicle does not meet the hypothesis of a circular hull shape. Because the surge and sway damping parameters are different, one of them must be chosen for the controller calculations. In this case, the smaller one β_u is chosen.

The controller is evaluated on a circular trajectory with the same $\boldsymbol{y_o}$-axis disturbing force as before. The circular trajectory has been chosen to showcase the behavior of the vehicle for all orientations and demonstrate that the singularity due to the arctangent function is of no consequence. The vehicle's position is initialized with a 15m error on the $\boldsymbol{x_o}$ axis.

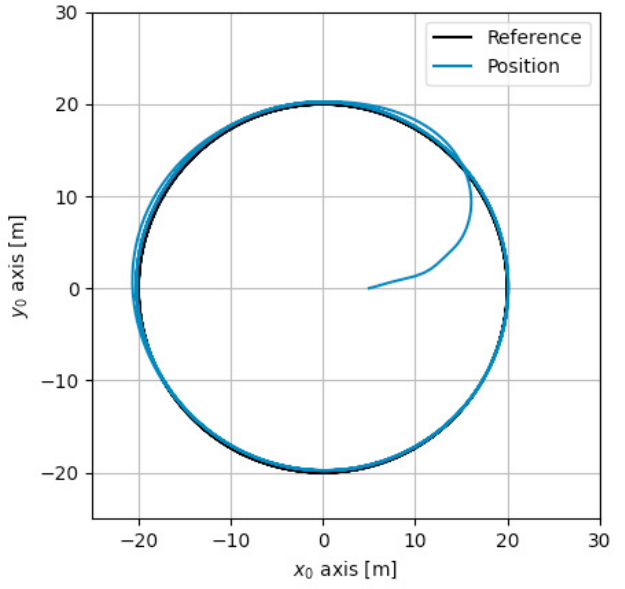

Fig. 6. Trajectory of the surface vessel in the $(\boldsymbol{x_o}, \boldsymbol{y_o})$ plane, in presence of a wind force aligned with the $\boldsymbol{y_o}$ axis. Black: Reference trajectory - Blue: Actual trajectory of the vehicle

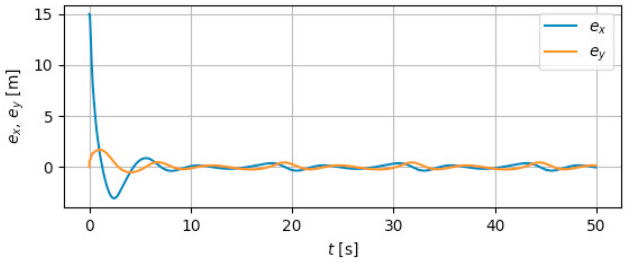

Fig. 7. Tracking errors of the surface vessel over time. Blue: Error on the $\boldsymbol{x_o}$ axis - Orange: Error on the $\boldsymbol{y_o}$ axis

Figs. 6 and 7 show that even with the consequent model approximation due to the shape of the surface vessel used in this example, the controller ensures convergence of the position of the vehicle towards the desired trajectory. Both errors are maintained very close to zero during all the application.

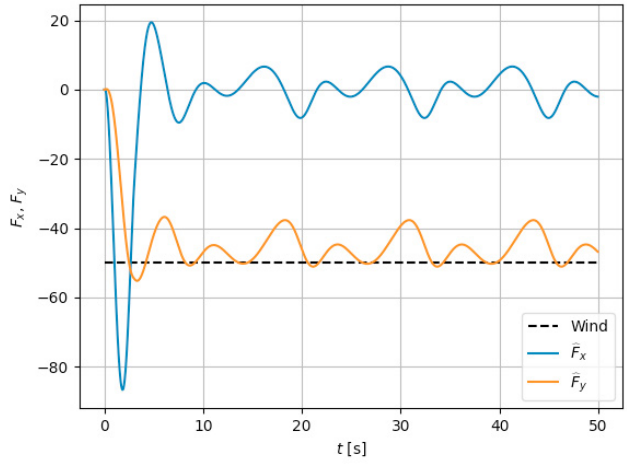

Fig. 8. Estimated values of F_x and F_y over time for the surface vessel. Dashed Black: Wind force - Blue: $\widehat{F}_x$ - Orange:$\widehat{F}_y$

Fig. 8 depicts the behavior of the two estimators on the surface vessel example. Both oscillate around the expected values: $\widehat{F}_x$ stays around zero and $\widehat{F}_y$ converges towards the wind value and oscillates around it. The oscillations observed on Fig. 8 are expected and demonstrate that the estimators of the iPDs also counteract the model approximations. In facts, one can observe two phase-shifted sinusoidal signals on the estimators curves. They correspond to the disturbances relative to the speed of the vehicle due to the error on the damping coefficient and the acceleration due to the approximation of the mass parameters.

Overall, our HEOL control setting, which associates a flatness-based guidance principle and a model-free regulator, shows very good performances on the circle trajectory when applied to this surface vessel even though it was calculated using the model of a hovercraft (compare with Sira-Ramírez (2002) and Rigatos (2015))

6. CONCLUSION

This work presents a novel approach to guidance and control of autonomous marine craft, via HEOL, which com-

bines flatness-based and model-free controls. Considering the hovercraft vehicle as a drastic simplification of the well-known surface vessel maneuvering model, a flatness-based guidance principle is established. The flatness of the hovercraft model gives equations of the surge force generated by the two parallel thrusters and of the heading angle of the vehicle that can be used as a guidance principle. Then, two decoupled model-free controllers relying on Intelligent PDs are used to close the loop. They add an additional layer of robustness to the controller, ensuring compensation of all external disturbing effects as well as compensating the model approximations due to usage of the hovercraft model. The controller has then been applied in simulation to a hovercraft and to a surface vessel with generic hull-shape and shows very good trajectory tracking results in both cases even in the presence of external disturbances. This work hints towards an all-purpose controller for marine craft based on the new promising HEOL standpoint.

REFERENCES

Artuedo, A., Moreno-Gonzalez, M., and Villagra, J. (2024). Lateral control for autonomous vehicles: A comparative evaluation. *Annual Rev. Contr.*, 57, 100910.

Breivik, M. and Fossen, T. (2005). Principles of guidance-based path following in 2D and 3D. *IEEE Conf. Dec. Contr.*, 627–634, Seville.

Degorre, L. (2023). *Analysis and Control of Autonomous Underwater Vehicles with Reconfigurable Vectoring Thrust.* Ph.D. Thesis, École Nat. Ingén. Brest.

Degorre, L., Delaleau, E., and Chocron, O. (2023). A survey on model-based control and guidance principles for autonomous marine vehicles. *J. Marine Sci. Engin.*, 11, 430.

Delaleau, E., Join, C., and Fliess, M. (2025). Synchronization of Kuramoto oscillators via HEOL, and a discussion on AI. *IFAC PapersOnLine*, 59-1, 229–234.

Delaleau, E., and Rudolph, J. (1998). Control of flat systems by quasi-static feedback of generalized states. *Int. J. Contr.*, 71, 745–765.

Elmokadem, T., Zribi, M., and Youcef-Toumi, K. (2016). Trajectory tracking sliding mode control of underactuated AUVs. *Nonlin. Dyn*, 84, 1079–1091.

Fliess, M. and Join, C. (2013). Model-free control. *Int. J. Contr.*, 86, 2228–2252.

Fliess, M., and Join, C. (2022). An alternative to proportional-integral and proportional-integral-derivative regulators: Intelligent proportional-derivative regulators. *Int. J. Robust Nonlin. Contr.*, 32, 9512–9524.

Fliess, M., Lévine, J., Martin, P., and Rouchon, P. (1995). Flatness and defect of non-linear systems: introductory theory and examples. *Int. J. Contr.*, 61, 1327–1361.

Fliess, M., Lévine, J., Martin, P., and Rouchon, P. (1999). A Lie-Bäcklund approach to equivalence and flatness of nonlinear systems. *IEEE Trans. Autom. Contr.*, 44, 922–937.

Fliess, M. and Sira-Ramírez, H. (2003). An algebraic framework for linear identification. *ESAIM: COCV*, 9, 151–168.

Fossen, T.I. (2021). *Handbook of Marine Craft Hydrodynamics and Motion Control* (2nd ed.). Wiley.

Fossen, T.I., and Perez, T. (2004). Marine systems simulator (MSS) - Matlab Toolbox.

Gédouin, P.-A., Delaleau, E., Bourgeot, J.-M., Join, C., Arbab Chirani, S., and Calloch, S. (2011). Experimental comparison of classical PID and model-free control: Position control of a shape memory alloy active spring. *Contr. Engin. Pract.*, 19, 433–441.

Hagenmeyer, V., and Delaleau, E. (2003a). Exact feedforward linearization based on differential flatness. *International Journal of Control*, 76(6), 537–556.

Hagenmeyer, V., and Delaleau, E. (2003b). Robustness analysis of exact feedforward linearization based on differential flatness. *Automatica*, 39, 1941–1946.

Join, C., Delaleau, E., and Fliess, M. (2024). Flatness-based control revisited: The *HEOL* setting. *C.R. Math.*, 362, 1693–1706.

Join, C., Delaleau, E., Fliess, M. (2025). Model-free predictive control: Introductory algebraic calculations, and a brief comparison with HEOL. *This Conference.* `arXiv:2502.00443`

Mitchell, A., McGookin, E., and Murray-Smith, D. (2003). Comparison of Control Methods for Autonomous Underwater Vehicles. *IFAC Proc. Volumes*, 36, 37–42.

Pettersen, K. and Nijmeijer, H. (1998). Tracking control of an underactuated surface vessel. In *IEEE Conference on Decision and Control*, volume 4, 4561–4566.

Rigatos, G.G. (2015). Differential flatness theory and flatness-based control. In G.G. Rigatos (ed.), *Nonlinear Control and Filtering Using Differential Flatness Approaches: Applications to Electromechanical Systems.* Springer.

Scherer, P., Othmane, A., and Rudolph, J. (2023). Combining model-based and model-free approaches for the control of an electro-hydraulic system. *Contr. Engin. Pract.*, 133, 105453.

Sira-Ramírez, H. (2002). Dynamic second-order sliding mode control of the hovercraft vessel. *IEEE Trans. Control Sys. Tech.*, 10, 860–865.

Sira-Ramírez, H. and Agrawal, S.K. (2004). *Differentially flat systems.* Marcel Dekker.

Appendix A

The elements of this Section follows Fossen (2021). The parameters m, I_z, $X_{\dot{u}}$, $Y_{\dot{v}}$ and $N_{\dot{r}}$ are respectively the mass, the moment of inertia, the surge, sway, and yaw added masses. Only linear decoupled damping is considered, d_u, d_v and d_r are the surge, sway, and yaw damping coefficients respectively. Finally, reduced parameters a, b, c, β_u, β_v and γ are introduced for ease of explanation. Moreover, τ_u is the surge force generated by the thrusters, τ_r is the yaw moment and F_u and Γ_r act as normalized inputs of the surface vessel model. The expressions of the parameters of model (1) are:

$$a = \frac{m - Y_{\dot{v}}}{m - X_{\dot{u}}}, \quad b = -\frac{1}{a}, \quad c = \frac{X_{\dot{u}} - Y_{\dot{v}}}{I_z - N_{\dot{r}}}$$
$$\beta_u = \frac{d_u}{m - X_{\dot{u}}}, \quad \beta_v = \frac{d_v}{m - Y_{\dot{v}}} \quad \gamma = \frac{d_r}{I_z - N_{\dot{r}}}$$
$$F_u = \frac{\tau_u}{m - X_{\dot{u}}} \quad \Gamma_r = \frac{\tau_r}{I_z - N_{\dot{r}}}$$

The hovercraft has a circular hull shape, consequently, the added mass parameters of the hovercraft are then equal in surge and sway: $X_{\dot{u}} = Y_{\dot{v}}$.